

Magnetism and Transport in Transparent High-Mobility BaSnO₃ Films Doped with La, Pr, Nd and Gd

Urusa S. Alaan,^{1,2,*} Franklin J. Wong,³ Jeffrey J. Ditto,^{4,5} Alexander W. Robertson,⁴ Emily Lindgren,^{1,2} Abhinav Prakash,⁶ Greg Haugstad,⁷ Pdraic Shafer,⁸ Alpha T. N'Diaye,⁸ David Johnson,⁵ Elke Arenholz,^{8,9} Bharat Jalan,⁶ Nigel D. Browning,^{4,10} and Yuri Suzuki^{2,11}

¹*Department of Materials Science and Engineering, Stanford University*

²*Geballe Laboratory for Advanced Materials, Stanford University*

³*Department of Materials Science and Engineering, University of California, Berkeley*

⁴*Physical and Computational Sciences Directorate, Pacific Northwest National Laboratory*

⁵*Department of Chemistry and Biochemistry, University of Oregon*

⁶*Department of Chemical Engineering and Materials Science, University of Minnesota*

⁷*Characterization Facility, University of Minnesota*

⁸*Advanced Light Source, Lawrence Berkeley National Laboratory*

⁹*Cornell High Energy Synchrotron Source, Cornell University, Ithaca, NY 14853, USA*

¹⁰*School of Engineering and School of Physical Sciences, University of Liverpool*

¹¹*Department of Applied Physics, Stanford University*

(Dated: November 4, 2019)

We have explored the effect of magnetic rare-earth dopants substitutionally incorporated on the Ba-sites of BaSnO₃ in terms of electronic transport, magnetism and optical properties. We show that for Ba_{0.92}RE_{0.08}SnO₃ thin films (where RE = La, Pr, Nd, Gd), there is a linear increase of mobility with carrier concentration across all doping schemes. La-doped films have the highest mobilities, followed by Pr- and Nd-doped films. Gd-doped samples have the largest ionic size mismatch with the Ba-site and correspondingly the lowest carrier concentrations and electron mobilities. However, crystallinity does not appear to be a strong predictor of transport phenomena; our results suggest that point defects more than grain boundaries are key ingredients in tuning the conduction of BaSnO₃ films grown by pulsed laser deposition. Pronounced, non-hysteretic x-ray magnetic dichroism signals are observed for Pr-, Nd- and Gd-doped samples, indicating paramagnetism. Finally, we probe the optical constants for each of the BaSnO₃ doping schemes and note that there is little change in the transmittance across all samples. Together these results shed light on conduction mechanisms in BaSnO₃ doped with rare-earth cations.

I. INTRODUCTION

A significant challenge in the field of oxide electronics over the last several decades has been the search for materials with high room-temperature carrier mobilities that can also be epitaxially integrated with complex oxides.¹⁻⁴ Several strongly correlated complex oxides configure themselves in the perovskite (ABO₃) crystal structure.³ Until recently, La-doped SrTiO₃ was among the highest mobility perovskite-structure oxides with $\mu \sim 53,200$ cm²/V·s at 2 K, but dropping to only ~ 7 cm²/V·s at 300 K.^{2,5} For this reason, the demonstration by Luo *et al.* that La-doped BaSnO₃ could have room-temperature mobilities higher than 100 cm²/V·s in bulk crystals attracted significant attention.⁶ Shortly thereafter, Kim *et al.* synthesized La-doped BaSnO₃ with room-temperature mobilities exceeding 300 cm²/V·s in bulk crystals; together these studies were a breakthrough in the field of oxide electronics.⁷⁻⁹ Thin films of La-doped BaSnO₃ have achieved $\mu \sim 180$ cm²/V·s by molecular beam epitaxy (MBE) on lattice-matched (110) DyScO₃ substrates and $\mu \sim 100$ cm²/V·s by pulsed laser deposition (PLD) when BaSnO₃ was grown homoepitaxially.⁹⁻¹² In addition to having a perovskite crystal structure and high carrier mobilities, La-doped BaSnO₃ is both transparent and colorless in the vis-

ible wavelength regime, even when it is degenerately doped.^{6,13}

The discovery of this new class of transparent conducting oxides unlocks new opportunities for applications ranging from thin-film transistor based displays to oxide photovoltaic systems. In addition, spintronic devices that require interfaces between metallic or semiconducting films and perovskite ferromagnets would benefit from the availability of lattice-matched materials. Moreover, the combination of three functional properties — low resistivity and high carrier mobility, optical transparency, and a magnetic moment — together in a single material would help to enable the realization of all-oxide spintronics platform for low-power, low-energy-consumption devices.

There have been several efforts toward doping transparent conducting oxides (TCOs) to make them ferromagnetic, with varying degrees of success. The focus of nearly all studies on magnetically doping BaSnO₃ has been on the incorporation of transition metals such as Mn, Fe and Co onto the BaSnO₃ lattice with substitution occurring on the Sn⁴⁺ site.¹⁴⁻²⁰ These compounds have generally exhibited ferromagnetic insulating behavior and are opaque in the visible wavelength range. If the ferromagnetism is intrinsic, it is hypothesized to result from an “F-center exchange” mechanism which re-

lies on oxygen vacancies that trap electrons and cause local ferromagnetic ordering.²¹ However, the need for charge carriers to be localized and strongly coupled to defect sites impedes their conduction. Efforts to codope BaSnO₃ with two transition metals on the Sn site to add both conduction and a magnetic moment have also resulted in insulating materials.²² Because electrical transport is governed by the conduction band with Sn 5s character, disruption of these B-sites causes both a loss of electrical conductivity as well as the occurrence of optical absorption in the visible regime. Furthermore, ferromagnetism itself is not reproducible across different studies, and d^0 magnetization is difficult to decouple from dilute transition-metal doping, intrinsic (e.g., phase segregation) and extrinsic (e.g., magnetic dust) contamination.^{19,20}

For these reasons, a more attractive route to designing a transparent, ferromagnetic semiconductor is through exploitation of the perovskite A-site, a degree of freedom in BaSnO₃ that is not accessible in binary TCO systems.^{19,23} Previously we demonstrated A-site doping of BaSnO₃ films with 4% Gd.²³ These films exhibit optical transparency and electron mobilities of 30 cm²/V·s at room temperature. While these Gd-doped films showed a strong paramagnetic signal at low temperatures, the magnetization was not hysteretic. The absence of ferromagnetism is likely due to two factors: an insufficient doping level, and a strongly localized wavefunction for Gd. In this study, we address both issues through dopant concentration and selection, respectively.

Long-range ferromagnetic order in ABO₃ perovskites is generally mediated by B–O–B indirect exchange interactions as A–O–A interactions are much weaker. Thus, if rare-earth doped BaSnO₃ were ferromagnetic, the coupling would be indirect because of the large distance between the magnetic impurities with low doping levels, as well as the localized nature of the 4f wave function. For this reason, Ruderman–Kittel–Kasuya–Yosida (RKKY) interactions may play a role in a system with a sufficient concentration of delocalized electrons, more so than oxygen-mediated exchange. In the 4f block, localization of the wave function increases with atomic number Z , so it could be advantageous to choose lower Z lanthanide dopants such as Pr and Nd. However, these also have fewer unpaired electrons than Gd, resulting in a lower moment overall. There is therefore a tradeoff in rare-earth dopant selection. Recently, McCalla et al. have demonstrated Pr- and Nd-doping of up to 0.5% in BaSnO₃ single crystals; these bulk samples showed good transport properties as well as paramagnetic behavior.²⁴ There have been also been recent studies of 7% Nd-doped BaSnO₃ films with metallic conduction but no report on magnetic response.²⁵

Toward developing optical and magneto-electric functionality in single material, we have doped BaSnO₃ (BSO) films with 8% Pr, Nd and Gd on the Ba sites. We have also synthesized 8% La-doped BaSnO₃ films as a control. This study shows the impact of dopant ionic

radii on the structure and transport properties, and also demonstrates that BaSnO₃ films can remain transparent at high concentrations of rare-earth doping. All films showed high electron mobilities and degenerate doping. Moreover, up to 8% Pr, Nd and Gd doping of BaSnO₃ gives rise to strong paramagnetic responses although no long-range order of dopant moments is observed.

II. EXPERIMENT

Thin films were grown by pulsed laser deposition (PLD) from sintered ceramic targets of Ba_{0.92}La_{0.08}SnO₃ (BLSO), Ba_{0.92}Pr_{0.08}SnO₃ (BPSO), Ba_{0.92}Nd_{0.08}SnO₃ (BNSO), and Ba_{0.92}Gd_{0.08}SnO₃ (BGSO). All targets were synthesized by Toshiba Manufacturing Company. An excimer laser (KrF, $\lambda = 248$ nm) was used to ablate the rotating targets with an energy density of ~ 1.4 J/cm². Growth of conducting samples was performed at 100 mTorr O₂ and 750 °C with a 2.5 inch distance separating the target from the (001) oriented single crystal SrTiO₃ substrates. Growth in poorer oxygen atmosphere (3.5×10^{-3} Torr) resulted in insulating samples albeit with similar crystalline quality to the conducting samples. The electronic properties of the samples were also particularly sensitive to the target-heater distance, with larger distances leading to more insulating films. The SrTiO₃ substrates were etched in hydrofluoric acid and annealed at 1000 °C, yielding TiO₂-terminated surfaces. While the termination itself was not important in this study, this etching procedure was conducted for the purpose of removing surface contaminants. Care was taken so that the samples were never handled with metal tweezers or any other ferromagnetic object.

Magnetometry was conducted in a Quantum Design Evercool Magnetic Property Measurement System (MPMS) with the reciprocating sample option (RSO). Samples were field-cooled in $H = +7$ T to 4.5 K before beginning measurements and the orientation of the field was always in the plane of the sample along the {100} type directions. A Quantum Design Physical Property Measurement System (PPMS) was used for current-sourced electrical transport experiments. Thin film samples were bonded with Al wire in a four-point geometry for van der Pauw and Hall effect measurements between ± 7 T. Optical properties and thicknesses were found from measurements on a J.A. Woollam M2000 spectroscopic ellipsometer with the depolarization option, and models were constructed using the corresponding WVASE32 software. Thicknesses were also deduced from Rutherford backscattering spectrometry (RBS), ellipsometry and x-ray reflectivity (XRR) for thinner samples. RBS was performed on a MAS 1700 pelletron tandem ion accelerator equipped with an analysis endstation and RBS data was analyzed with SIMNRA software. A Panalytical X'Pert diffractometer with a Cu K _{α 1} source was used for x-ray diffraction (XRD) and x-ray reflectivity (XRR) measurements. Surface morphology was studied by atomic

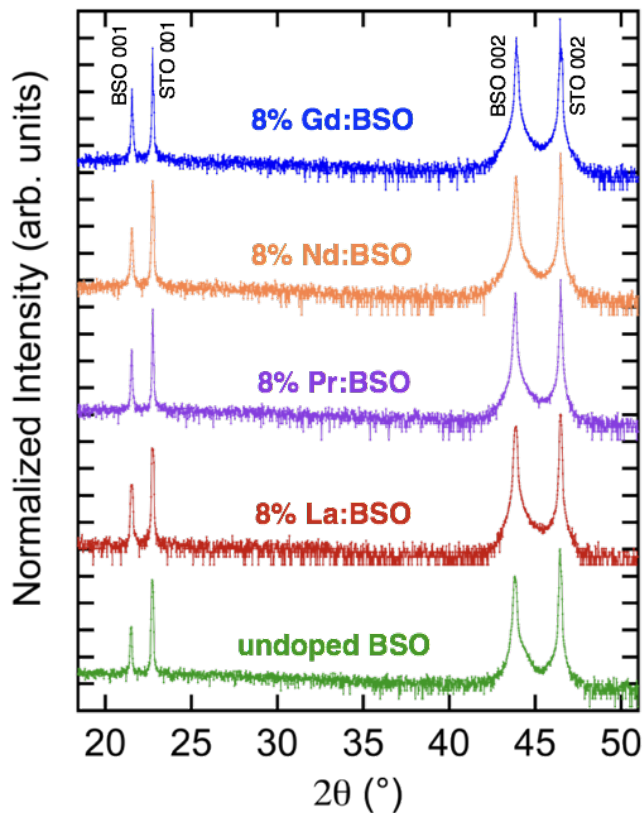


Figure 1. X-ray diffraction spectra of 8% Gd-, Nd-, Pr- and La- doped BaSnO_3 films as well as undoped BaSnO_3 films. The out-of-plane lattice parameter decreases toward the bulk value as the Ba site dopant decreases in ionic radius. The spectra are normalized by substrate intensity and shifted for clarity.

force microscopy (AFM) using a Digital Instruments Dimension 3100 tool. X-ray absorption (XAS) and x-ray magnetic circular dichroism (XMCD) measurements were conducted at the Advanced Light Source (ALS) using Beamlines 4.0.2 and 6.3.1 in total electron yield mode (TEY) at a 30° grazing angle of incidence.

III. RESULTS

A. Structure

All the doped films grown at 750°C , 100 mTorr O_2 and 2.5 inch target-to-substrate distance show similar structural properties. Representative $\theta - 2\theta$ spectra as measured by x-ray diffraction are given in Figure 1. Despite the large lattice mismatch of the films ($a = 4.117 \text{ \AA}$ for bulk BSO) on the underlying (001) SrTiO_3 substrates ($a = 3.901 \text{ \AA}$), they are epitaxial and of good structural quality.^{3,11} When grown thin enough, they show Kiessig fringes in x-ray reflectivity and Laue oscillations around the 002 Bragg reflection.²⁶ The films were highly crystalline with a typical rocking curve full-

Table I. Out-of-plane lattice constants for 8% rare-earth doped films as determined by x-ray diffraction. The FWHM of the rocking curves around the 002 Bragg reflection ($\Delta\omega$) are also given. The effective ionic radii of the dopants in a 12-fold coordination ($R_{i,12}^{3+}$) are used to calculate the A-site site mismatch as compared to Ba^{2+} ($r = 1.61 \text{ \AA}$ by Shannon).^{27,28} The calculated ionic radii for the rare-earth cations are from Jia (1991).²⁹

Dopant	a_{OOP} (\AA)	$\Delta\omega_{002}$ ($^\circ$)	$R_{i,12}^{3+}$ (\AA)	Site mismatch
La^{3+}	4.128 ± 0.004	0.060 ± 0.071	1.36	15.5%
Pr^{3+}	4.127 ± 0.003	0.039 ± 0.010	1.32	18.0%
Nd^{3+}	4.124 ± 0.004	0.073 ± 0.089	1.31	18.6%
Gd^{3+}	4.120 ± 0.004	0.041 ± 0.029	1.27	21.1%

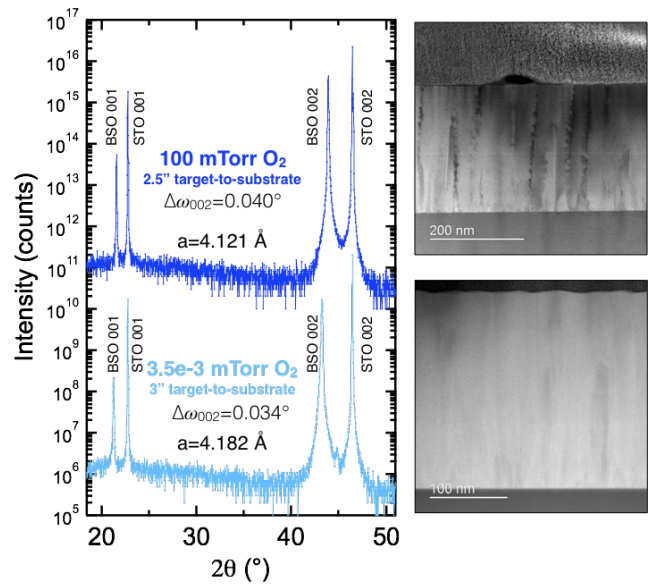


Figure 2. Comparison between the structural quality of two 8% Gd-doped BaSnO_3 films that exhibit vastly different electronic transport. The top sample is conducting with $\mu = 12.2 \text{ cm}^2/\text{Vs}$ and $\rho = 5.4 \text{ m}\Omega$, while the bottom sample is too insulating to measure in our transport system. The XRD spectra have been normalized by substrate intensity and shifted for clarity.

width-at-half-maxima of $\Delta\omega_{002} \sim 0.04^\circ$. Table I gives the out-of-plane (OOP) lattice parameters (a_{OOP}) as well as rocking curve full-width-at-half-maxima ($\Delta\omega_{002}$) measured around the 002 Bragg reflections for films with thicknesses between 270-300 nm. Lattice constants for all doped films are shown in Supplemental Section 1.

It is evident that there is quite a large mismatch between the rare-earth cation sizes and the host barium site; for Gd^{3+} the size difference is over 20%. And yet for all rare-earth doping cases, including gadolinium, there is a slight *increase* of the lattice parameters from that of undoped BaSnO_3 bulk ($a = 4.117 \text{ \AA}$)³⁰ as shown in Table I. It appears that the presence of charged defects serves to expand the lattice due to Coulombic repul-

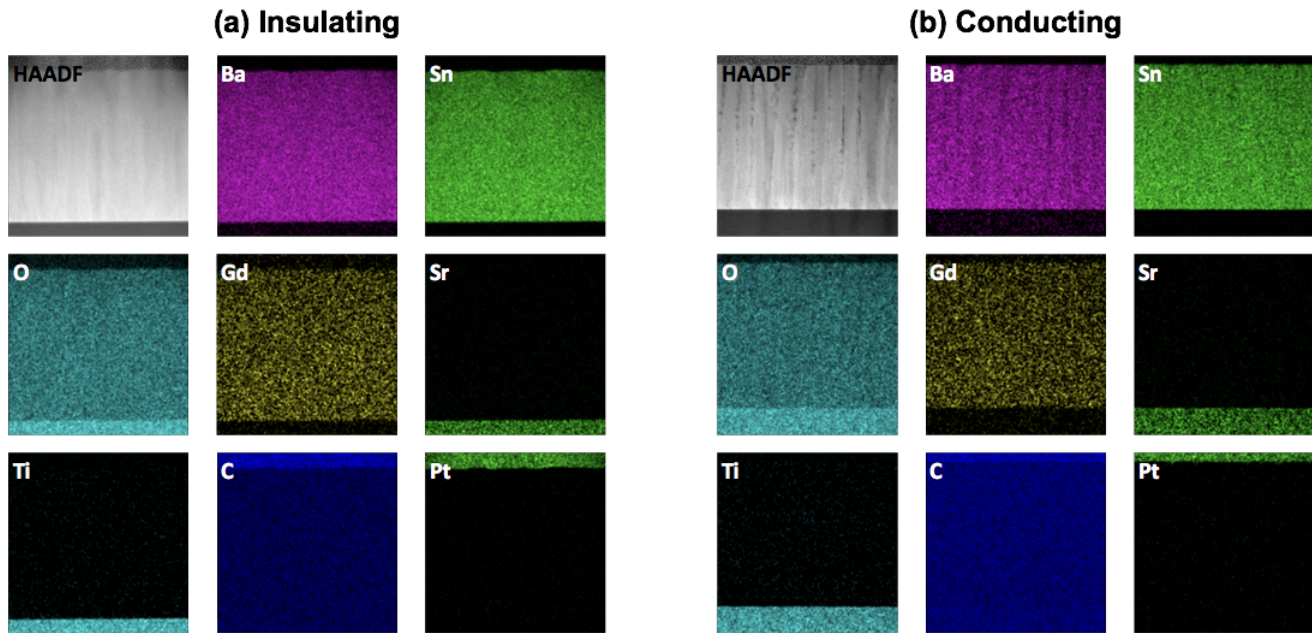


Figure 3. Energy-dispersive spectroscopy of both the (a) ‘insulating’ and (b) ‘conducting’ 8% Gd-doped BaSnO_3 films measured in cross-sectional TEM show homogeneous incorporation of the dopant atoms.

sion effects. This is also consistent with the results on La-doped BaSnO_3 in literature.^{7,23,27,28,31,32} As we dope with higher percentages of RE^{3+} species, the overall lattice will expand as a result of charged point defects on the cation sublattice. This is counteracted by having substitutional dopants that are smaller than their host site, and so we only see a small increase in the lattice parameter in our doped BaSnO_3 films. From La-doping to Gd-doping, there is a slight change in the lattice constant of only about 0.2%. Since both dopants are trivalent, this further indicates that the lattice constant is more a function of defect concentration than substitutional cation size in these films.

PLD growth at different conditions can lead to films with comparable crystallinities (as determined by the rocking curve widths), but with vastly different functional properties. In early studies, La dopants had been incorporated into BaSnO_3 crystals of high quality, but high mobilities had not been achieved.^{30,33–41} The newest wave of studies also shows a large variation in properties with the same nominal stoichiometries across different groups, and sometimes even within the same group.^{7–9,32,42–51} We have found that microstructure alone is not always a good indicator of carrier mobilities in PLD-grown films.^{10,11,46,52}

Three parameters that had a significant impact on the resulting film properties were PLD target-to-substrate distance, oxygen growth pressure, and substrate choice. The target-to-substrate distance in PLD appears to strongly affect electrical transport in the resulting films. While generally it is preferable to keep the substrates further away from the high-energy plume in order to avoid

re-sputtering of the film surface, we found that at distances of 3 inches, the conduction turned off entirely. All of the films for which transport is shown in this study were grown at distances of 2.5 inches. Next, we found that the ambient growth environment strongly influenced the conductivity, with high mobilities achieved at 100 mTorr O_2 . Below 2 mTorr of oxygen, the films were quite insulating. Growing in oxygen pressures of 10^{-5} Torr led to high-quality films with low rocking curve widths, but even heavily-doped BaSnO_3 films were insulating. Holding pressure constant at 100 mTorr but flowing a mixture of 99% N_2 /1% O_2 instead of pure O_2 also yielded completely insulating films. This is somewhat surprising because oxygen vacancies should in theory be n-type dopants and it has been shown that if undoped BaSnO_3 films are post-annealed in vacuum, they can be made conducting.^{49,53} The fact that growth in low oxygen pressures turns the conductivity off in PLD suggests that there are other compensating defects or unintended consequences to changing the growth pressure. Finally, we compared depositions on (001) SrTiO_3 substrates to those on (001) MgO substrates. While the difference between the rocking curve breadths of the films was very large — 0.03° to 0.7° , respectively — there was virtually no difference in the electron mobilities.

This lack of correlation between microstructure and electronic properties suggests that either the dopants were not incorporated into the samples or there were significant compensating defects such as cation vacancies or antisite defects. In order to investigate this further, we compared two Gd-doped films that had approximately the same full-width-at-half-maxima of their rock-

ing curves but which had very different electronic transport properties. In this section, we will refer to them as the ‘conducting’ film and the ‘insulating’ film. The ‘conducting’ film used the recipe outlined previously — a 2.5 inch target-to-substrate distance and an ambient pressure of 100 mTorr O_2 . The ‘insulating film’ was grown at a 3 inch target-to-substrate distance and an O_2 pressure of 3.5×10^{-3} mTorr. The temperature was held constant at 750 °C and (001) $SrTiO_3$ substrates were used in both cases. The out-of-plane x-ray diffraction spectra are given in Figure 2. Both show comparable crystallinity, with $\Delta\omega_{002} = 0.040^\circ$ for the conducting film and $\Delta\omega_{002} = 0.034^\circ$ for the insulating film. There is an expansion of the lattice parameter for the insulating case, perhaps as a result of additional charged defects such as oxygen vacancies.

The right-hand side of Figure 2 shows the cross-sectional transmission electron microscopy (TEM) images for both films. Both show columnar grains; however in the conducting sample there are large voids between the grains with a grain size of approximately 30-50 nm. These voids appeared to be deficient in both Ba and O. The surface quality was also quite different in both samples. The conducting films have patches of surface contrast at low magnifications that EDS identifies as barium oxide islands, whereas the insulating film appeared homogeneous even at higher magnifications. In both films, there were frequently lamellar defects that appeared as bright lines of contrast in dark-field imaging. Upon further inspection, they seemed to be regions of varying thickness in parts of the sample where islands that had nucleated separately began to impinge on one another.

We conducted energy-dispersive spectroscopy (EDS) in conjunction with cross-sectional TEM as shown in Figure 3. Despite their very different electrical properties, both films had rare-earth dopants that were evenly interspersed throughout the samples. Thus, the lack of free carriers in the insulating film was not the result of dopant clustering or a lack of incorporation. In some cases, there were BaO islands on the surface of the conducting films, and Sn coated the voids between the grains as shown in Supplemental Section 2. No such features were observed in the insulating films. It is surprising that the film with (slightly) higher $\Delta\omega$ values and with extensive microstructural defects as seen in TEM can have the excellent transport properties that will be discussed in Section III B.

B. Electronic transport

All of the dopants tested in $BaSnO_3$ were n-type, yielding high room-temperature mobilities and conductivities when grown in 100 mTorr O_2 and with a 2.5 inch target-to-substrate distance. Only films grown in oxygen-poor ambient conditions or at larger target-to-substrate distances are insulating. The doped BSO films are metal-

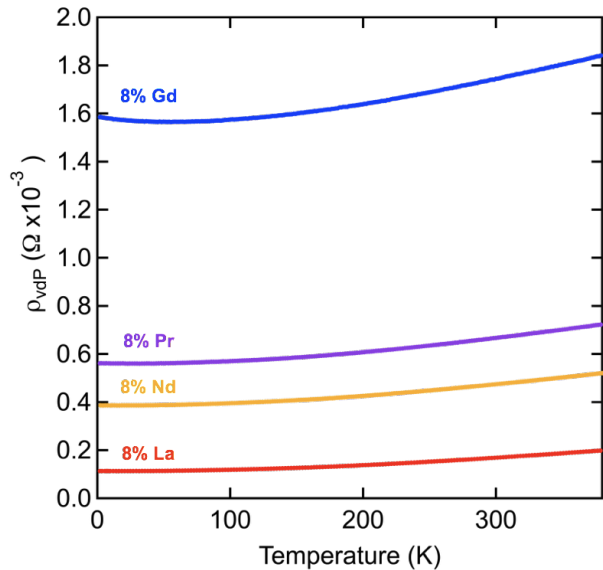


Figure 4. Resistivity versus temperature for a few representative 8% Pr, Nd and Gd-doped $BaSnO_3$ films in Figure 5.

lic (i.e., $\frac{d\rho}{dt} > 0$) across the temperature range 2-380 K; however, the resistivity versus temperature curves are still quite flat as shown in Figure 4. This indicates that phonon scattering does not play an important role in the transport of these films and that scattering from ionized impurities is the dominant mechanism limiting the resistivity. This is consistent with other reports in the literature, where degenerately-doped $BaSnO_3$ is not significantly affected by changes in temperature.^{10–12,25} All films do exhibit a flattening of the resistivity curve and a slight upturn at lower temperatures. This has also been observed across multiple studies on the $BaSnO_3$ system and is sometimes attributed to weak localization. In our case, the increase in resistivity is coincident with a decrease in carrier concentration. All films exhibit a small negative magnetoresistance, measured with the applied field perpendicular to the sample plane, at low temperatures. This behavior can arise from the presence of strong paramagnetic moments.

Of the dopants in this study, La-doping of $BaSnO_3$ resulted in the highest mobilities, with values as high as $65 \text{ cm}^2/\text{V}\cdot\text{s}$. As the ionic radii of the dopant species decreases from La down to Gd (see Table I), the typical mobility values correspondingly decrease despite the films having similar crystalline quality. One likely explanation is that the larger the site mismatch with the native Ba site, the more pronounced the local strain fields which would serve to limit the carrier mobilities. Different activation energies may also account for this behavior. Typical room temperature mobilities for La, Pr, Nd and Gd-doped $BaSnO_3$ films are shown in Figure 5 and tabulated in Table II.

All of the rare-earth doped samples appear to lie along the same carrier concentration (n) versus mobility (μ)

Table II. Representative transport properties for each doping scheme.

Dopant 8%	ρ_{300K}^{vdP} ($m\Omega\cdot cm$)	μ_{300K} ($cm^2/V\cdot s$)	n_{300K} ($10^{20}cm^{-3}$)	ℓ (nm)
La	0.169	63.3	5.85	11
Pr	0.484	34.0	3.80	5.0
Nd	0.477	34.7	3.77	5.1
Gd	1.74	20.2	1.78	2.3

curve as the La-doped samples although with lower mobilities and carrier concentrations overall. They are well-segregated by n , so fewer carriers seem to be activated with higher- Z (lower ionic radius) dopants. The Gd-doped samples are clustered in the bottom-left corner of the plot, with the lowest mobilities and carrier concentrations. As we noted previously, Gd^{3+} has the greatest size mismatch with the host Ba^{2+} site. This could lead to local strain fields around the A-sites and cause a decrease in mobility. Another possibility is that with smaller cations, there is a greater probability of B-site occupation. Scanlon has calculated that after oxygen vacancies, anti-site defects have the lowest formation energies in $BaSnO_3$.⁵⁴ Therefore antisite disorder is a possible explanation. Similar arguments can be made for Pr- and Nd-doped samples as compared to La-doped samples.

Other reports on doped $BaSnO_3$ thin films also show a positive trend between carrier concentration and mobility.^{10–12,55} This correlation indicates that grain boundaries and dislocations that are introduced concurrently with aliovalent dopants serve to both scatter and trap carriers simultaneously. That is, there may be a screening effect that occurs within the material; once dislocations are sufficiently compensated through trapping of electrons, additional carriers added to the system may scatter from impurities, but the defects have already been compensated so there is no loss to mobility with increased carrier concentration.

Given that we have found that our films have a small grain size on the order of 30-50 nm, we can compare this with the mean free path as calculated from $\ell = v_{FT}\tau = \frac{\hbar\mu}{e}(3\pi^2n)^{1/3}$. The calculated mean free paths are given in Table II. For the La-doped sample, ℓ is about a third of the grain size, while for Gd-doping, the mean free path is an order of magnitude smaller than the grain size measured by TEM. These mobilities are then reasonable values. Furthermore it explains why larger grain sizes do not significantly impact electrical transport in these films. Together these results suggest that point defects and ionized impurities are more relevant to mobility-limiting mechanisms than grain-boundary scattering.

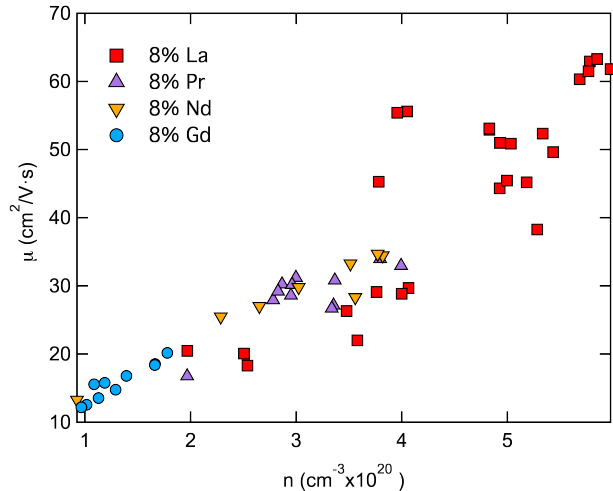


Figure 5. Mobility versus carrier concentration for 8% Pr, Nd and Gd-doped $BaSnO_3$ films at room-temperature. All films in this plot have thicknesses of approximately 300 nm.

C. Magnetism

We probed the magnetic response of the films using SQUID magnetometry and x-ray magnetic circular dichroism. In order to minimize the possibility of having spurious signals on the order of the intrinsic magnetic moment (i.e., due to magnetic dust or other extrinsic impurities), the films measured by SQUID magnetometry were grown to thicknesses of $\sim 3 \mu m$. Magnetic moment versus field curves are given in Figure 6 for 8% Pr, Nd and Gd doping schemes. Samples were field-cooled from room-temperature in 7 T and measured at 4.5 K. In each of the curves, there is a strong paramagnetic signal with a characteristic S-shaped curve.

We modeled the magnetization in these samples in terms of non-interacting spins as described by $M = M_s \cdot B_J(y)$ where $M_s = ng_J\mu_B J$, where $B_J(y)$ is the Brillouin function, n is the number of magnetic moments per unit volume, J is the angular momentum, and g_J is the Landé g-factor $g_J = \frac{3}{2} + \frac{S(S+1) - L(L+1)}{2J(J+1)}$. The Brillouin functions for the trivalent dopant ions are plotted in green in Figure 4. We set the function to match the magnitude of the data at 7 T, and fit for the first derivative. The shape of the magnetic response is well-described by this relation for the Nd^{3+} and Gd^{3+} cases. However, the measured data falls short of the predicted Pr^{3+} response. The slope about the origin is better described by the Pr^{4+} function (given by the red line in Figure 4, which is a $4f^1$ system). While most of the rare-earth ions are trivalent, both Pr^{4+} with an electron configuration of $4f^15d^06s^0$ and Pr^{3+} with $4f^25d^06s^0$ are stable depending on the surrounding environment. For example, $PrCoO_3$ is primarily in a Pr^{3+} valence state but below its spin state transition there is a charge transfer between the cations resulting in a detectable amount of

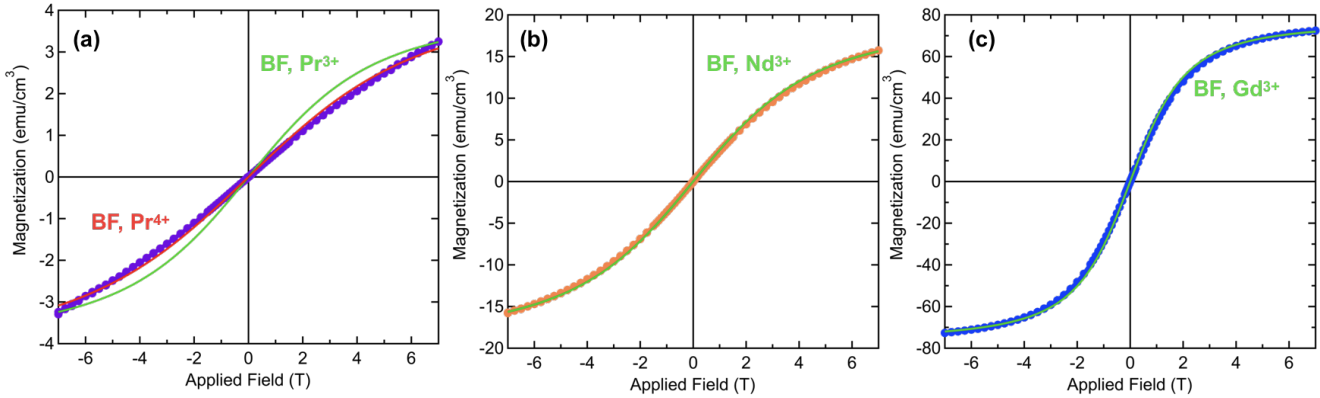


Figure 6. SQUID magnetometry results at 4.5 K for (a) 8% Pr, (b) 8% Nd and (c) 8% Gd-doped BaSnO₃. The green lines represent the Brillouin functions for the trivalent ions. In (a), both the trivalent (Pr³⁺, green) and tetravalent (Pr⁴⁺, red) cases are plotted.

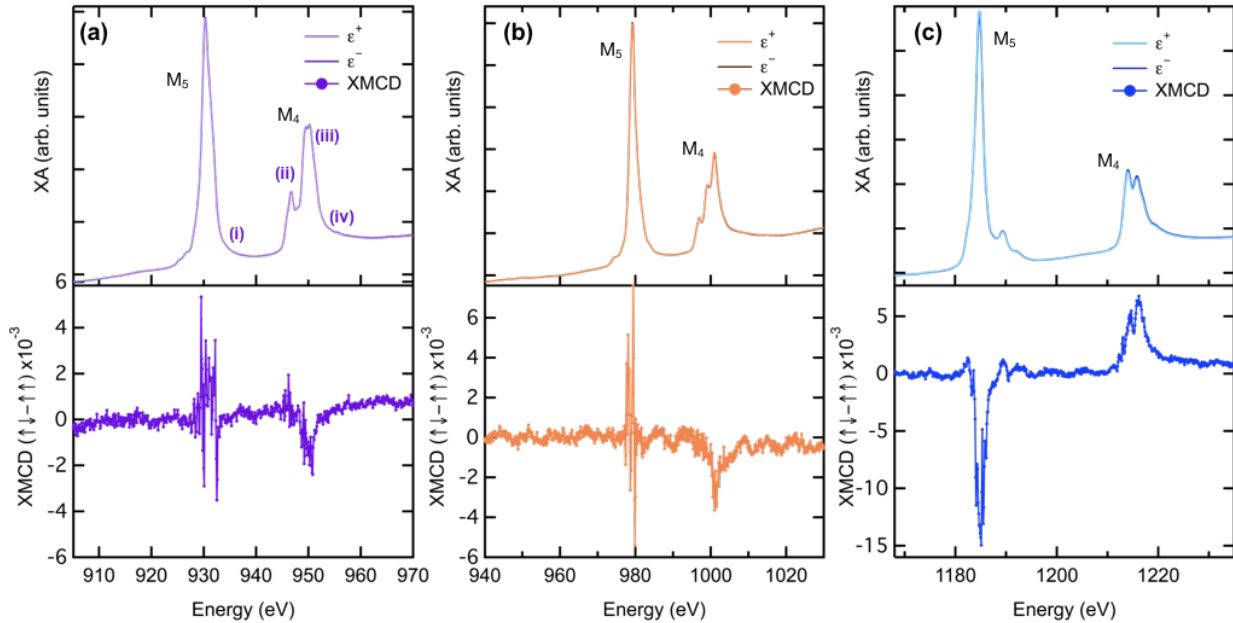


Figure 7. X-ray absorption and x-ray magnetic circular dichroism measurements at ~ 20 K on (a) Pr M_{45} edge for 8% Pr, (b) Nd M_{45} edge for 8% Nd and (c) Gd M_{45} edge for 8% Gd-doped BaSnO₃ films. The lower energy peak for all samples is the M_5 while the higher-energy XAS peak corresponds to the M_4 transition. Measurements were conducted on Beamline 4.0.2 of the Advanced Light Source with an applied magnetic field for XMCD measurements of ± 0.5 T.

Pr⁴⁺ in the x-ray absorption spectroscopy spectra.^{56–59} Pr can also be found on the B site in an octahedral environment. BaPrO₃ is a stable compound that can exhibit long-range magnetic order arising from exchange between Pr⁴⁺ cations.^{60,61} It has also been shown that when Pr is doped into BaXO₃-type compounds, it can be tetravalent and occupy the X-site. Hinatsu *et al.* showed that BaCeO₃, BaZrO₃, BaHfO₃ and even BaSnO₃ can each have Pr⁴⁺ substitutionally dope the tetravalent B-site. This isovalent doping scheme leads to an increase of the lattice parameter.^{62–64}

In order to investigate whether there is evidence for

Pr⁴⁺ in our doped BaSnO₃ samples, we conducted x-ray absorption spectroscopy (XAS) and x-ray magnetic circular dichroism (XMCD) experiments at ~ 20 K around the rare-earth $M_{5,4}$ edges as shown in Figure 7. The M -edges probe transitions from the $3d$ states to the unoccupied $4f$ levels. Comparing experimental reference spectra for Pr³⁺ and Pr⁴⁺, we see that the peaks in Figure 7(a) near the (ii) and (iii) markers are indicative of Pr³⁺ on the perovskite A-site in oxides. Pr⁴⁺ in an octahedral environment gives broad features at energies corresponding to (i) and (iv) in BaPrO₃.^{56,59} While we do not see any notable signatures at (i), there is a small feature at

(iv) in our data which is consistent with some amount of Pr^{4+} in the Pr-doped samples. XAS is also surface-sensitive technique, and therefore would not be able to detect to Pr^{4+} deeper within the film. The XAS features observed in the Nd and Gd-doped samples are very similar to calculated spectra for the trivalent state.⁶⁵⁻⁶⁷

A nonzero XMCD signal was observed in all samples on the $M_{4,5}$ edges of the lanthanide dopants. All measurements were taken at ± 0.5 T and are given in the ($\uparrow\downarrow - \uparrow\uparrow$) convention; the change in sign of the XMCD signal from Pr and Nd to Gd is a result of differences between half-filled and less than half-filled orbitals. For rare-earth elements with the $4f$ less than half-filled, $J = |L - S|$; however, for rare-earth elements with the $4f$ half-filled or more than half-filled (Gd and above), $J = |L + S|$. This is reflected in calculations by Goedkoop and others.^{66,67} The larger XMCD signal for the Gd-doped sample is a result of a greater difference between spin-up and spin-down transition probabilities in Gd. Since Gd^{3+} is a $4f^7$ system, each of the 7 electrons is unpaired and will minimize their energy if they have the same spin. Due to the weaker signal of Pr^{3+} and Nd^{3+} , some fluctuations in the background intensity of the XMCD spectra are observable. (These are artifacts and do not correspond to actual transitions.) Magnetic field loops between ± 0.5 T were taken on the M_5 edge, and exhibit no observable hysteresis in the XMCD.

Together these results suggest that our Pr-, Nd- and Gd-doped BaSnO_3 samples are paramagnetic with no long-range magnetic ordering. In the case of Pr-doping, there is evidence to suggest that the films may have some quantity of Pr^{4+} , which would serve to reduce the observed magnetic signal. In the case of our Nd-doped samples, we believe the BaSnO_3 is doped with Nd^{3+} on the Ba site. While there are some reports in the literature that Nd can be divalent, our spectra contain all of the features of Nd^{3+} and our SQUID results are well-fit by assuming contribution to the signal only from trivalent cations. In our Gd-doped samples, the spectral shape of the Gd M-edge is very similar to other Gd^{3+} -containing compounds. Furthermore, the Brillouin function for Gd^{3+} describes the SQUID magnetometry field dependence quite well.

D. Optical properties

The optical properties of the films were measured using ellipsometry. The dielectric constant ϵ_2 for a SrTiO_3 substrate and an 8% La-doped BaSnO_3 film on a SrTiO_3 substrate are plotted in Figures 8*ab*. Models for interpretation of ϵ_2 were built using Woollam's WVASE32 software. Each model consisted of Drude and Tauc-Lorentz 'oscillators', or functional forms, in series to describe the predicted response from the Fresnel equations which depend on the optical constants and the thickness of the materials. These oscillators are plotted as dashed lines in Figures 8*a* and *b*. For the SrTiO_3 substrate, there are

some deviations from ideal SrTiO_3 , which is compensated by adding a third Tauc-Lorentz oscillator with a broad functional form.

The shape of ϵ_2 is quite different for 8% La-doped BaSnO_3 compared to the substrate. The conducting films show a significant Drude tail at low energies as a result of introducing free carriers into the material, an observation that is consistent with our electrical transport results. The first band-to-band transition in the 8% La-doped film occurs at a higher energy than in SrTiO_3 and is also weaker in intensity. This likely stems from the lower density of states for the $5s$ -derived conduction band, as compared to the $3d$ conduction band in SrTiO_3 . The Sn $5s$ has a lower band degeneracy than the Ti $3d$; since we are essentially probing the probability of transition from the O $2p$ to the conduction band, the intensity of ϵ_2 will be higher for transition metal oxides than for compounds that have conduction bands with strong s character.

We also notice that the onset of absorption in BaSnO_3 occurs at higher energies than for SrTiO_3 , indicating that BaSnO_3 has a larger band gap than the substrate. This is consistent with the literature, where SrTiO_3 is reported to have a band gap of approximately 3.2 eV and BaSnO_3 is reported to have a band gap in the range of 3-4 eV.^{6,42,68-70} Since the substrate is more strongly absorbing than the film in this system and also has more features, it is useful to derive the transmittance from reflection measurements (as with ellipsometry) rather than from transmission measurements (as with UV-VIS spectroscopy). For this reason, we have calculated the transmittance for the doped BSO films only by subtracting the contribution from the underlying SrTiO_3 substrate.

Transmittance curves for 200 nm doped freestanding BaSnO_3 films alone are calculated from the extracted BSO optical constants and shown in Figure 8*d*. The oscillations are a function of film thickness. There are no notable differences between the transmittance of films with different rare-earth dopants. All are fairly transparent across the visible range despite being quite thick and degenerately doped.

IV. DISCUSSION

In our films, we find that microstructural quality is not a good predictor of conductivity. Instead, growth conditions such as oxygen pressure and target-to-substrate distance play a dominant role in determining the electrical transport of the films. Since microstructure is not the limiting factor in the conductivity, point defects likely cause the vast changes in mobility, carrier concentration and resistivity values. Not only have we found that microstructure does not track neatly with transport, but we also show through TEM with EDS that dopants can be well-dispersed throughout samples without leading to any measurable conduction. Electrical conduction can be completely turned off simply by decreasing the oxygen pressure or changing the target-to-substrate

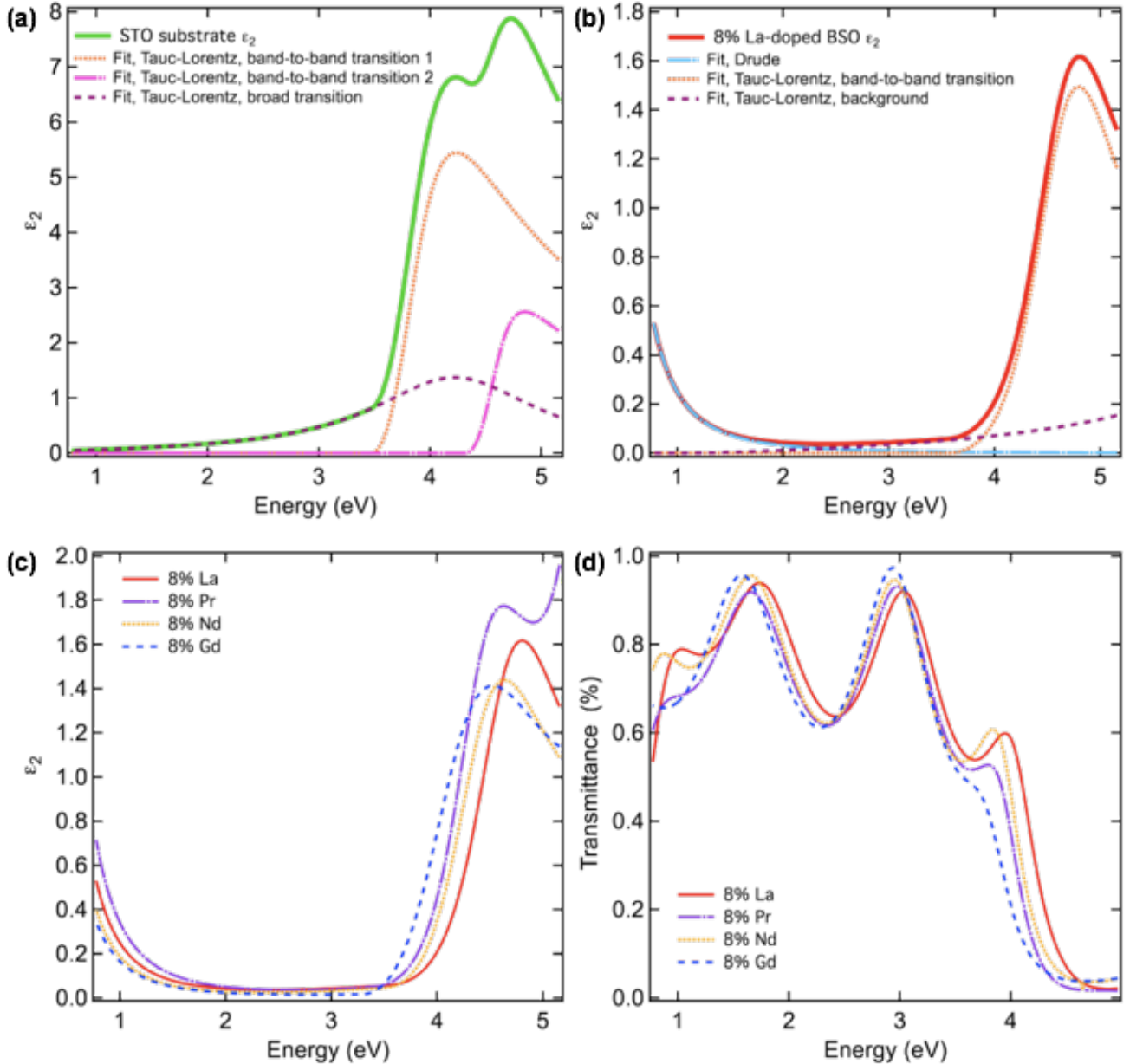


Figure 8. Optical properties of the SrTiO₃ substrate and doped BaSnO₃ films. (a) ϵ_2 of the SrTiO₃ substrate with the oscillators used to construct the model. (b) ϵ_2 of an 8% La-doped BaSnO₃ film with individual model components shown. (c) ϵ_2 for the same 8%-doped La film compared with films doped with 8% Pr, 8% Nd, and 8% Gd. (d) Transmittance for freestanding BaSnO₃ 200 nm films as calculated from optical constants.

distance. Together with literature on BaSnO₃ prior to 2012, our study offers further evidence that point defects are affecting the transport in ways that are difficult to detect.^{30,33–41}

When a trivalent rare-earth (RE) element substitutes for Ba²⁺, there *must* be some way to maintain crystal neutrality. In the ideal case RE_{Ba}[•] is compensated by delocalized electrons (e[']), but there are other negatively charged defects that could form instead. Negatively charged defects that in theory could form in doped BaSnO₃ films are oxygen interstitials (O_i[']), cation vacan-

cies (V_{Ba}['], V_{Sn}[']), and antisite defects (Ba_{Sn}[']). Site mixing of rare-earth dopants could also play a role in parasitic compensation (e.g., Gd_{Sn}[']). For completeness, we list possible positively-charged defects that could potentially enhance n-type conduction or screen negatively-charged point defects: V_O^{••}, Ba_i^{••}, Sn_i^{••••}, Sn_{Ba}^{••}, RE_i^{••••}, RE_{Ba}[•]. We note that we also conducted XAS on the oxygen K-edge for these doped BaSnO₃ films, but did not detect any major change in the lineshape between conducting and insulating films, or between La, Pr, Nd and Gd doping schemes. (See Section 3 of the Supplementary informa-

tion.)

We consider each of the proposed negatively-charged defects individually. While it has been calculated that oxygen interstitials actually have low formation energies in BaSnO_3 , it is predicted that they will relax toward lattice oxygen sites and form local peroxide groups.⁵⁴ Higher oxygen pressures during growth actually aid conduction in our case and O_i'' are acceptor-like defects. For this reason, cationic vacancies are a more likely scenario. Prakash *et al.* (2017) deliberately engineered barium vacancies in their highly conducting films grown by hybrid-MBE.⁵² In our TEM and EDS results, we see that there are BaO islands on the surface of the conducting films but not the insulating ones (Supplementary section 2). So, it seems likely that V_{Ba}'' could occur. However, Scanlon (2013) reports that in theory, oxygen-rich conditions serve to compensate n-type conduction.⁵⁴ We observe the opposite case; higher oxygen pressures are *more* likely to stabilize n-type conducting films. Still, the basic premise that V_{Ba}'' is a low-energy defect may be relevant. In terms of V_{Sn}''' , Coey *et al.* and others have reported that Sn is a volatile species in pulsed laser deposition, and that the target-to-substrate distance can influence the incorporation of Sn.^{21,71} Since closer target-to-substrate distances lead to higher conductivities and potentially more Sn, V_{Ba}'' may play a role in the insulating nature of films grown with large target-to-substrate distances. Finally, we consider the antisite defect Ba_{Sn}'' . Solely predicated on size considerations, there is a large mismatch between these dopants. 12-fold coordinated Ba^{2+} has an ionic radius of 1.61 Å while octahedrally coordinated Sn^{4+} has an ionic radius of 0.69 Å. In a strictly stoichiometric compound, occurrence of Ba_{Sn}'' may be unlikely. However, it has been reported that due to the large size of the A-site in BaSnO_3 , the Sn cations may actually reside on the A-sites and take a divalent oxidation state to form $\text{Sn}_{\text{Ba}}^{\times}$.^{35,39,54,72} While the defect itself is charge-neutral, site balance requirements can induce charged cationic vacancies, thereby suppressing conductivity in our doped films.

Another puzzling feature of our findings is that growth in low oxygen pressures by PLD suppresses conductivity, even though it has been theoretically predicted that oxygen vacancies are an n-type dopant, and experimentally shown that post-growth annealing in vacuum can lead to conduction and high electron mobilities.^{49,53,54} Clearly, growth by PLD in low oxygen pressures has unintended consequences. The need for high growth pressures as well as a close target-to-substrate distance suggests that in PLD growth of BaSnO_3 , the region of the plume that is sampled by the substrate is critical to generating the point defects that lead to conduction instead of compensating species.

Finally, we consider the differences in conduction between different dopants in our study. La-doping clearly leads to the most desirable transport properties for traditional uses of transparent conducting oxides. The PLD-grown La-doped samples have the highest mobil-

ities of the samples in this study, reaching as high as $\mu = 65 \text{ cm}^2/\text{V}\cdot\text{s}$ at room temperature. They are thus comparable to existing literature on La-doped BaSnO_3 films grown by pulsed laser deposition^{4,8,55} although films grown by molecular beam epitaxy have shown higher electron mobilities.¹⁰⁻¹² Gd-doping leads to the lowest conductivities and mobilities. It may be that the size mismatch between Gd^{3+} and Ba^{2+} causes the rare-earth to preferentially sit on the Sn^{4+} sites. Then, Gd_{Sn}' could compensate $\text{Gd}_{\text{Ba}}^{\bullet}$. In the La-doped system, theoretical predictions do suggest that under some circumstances,⁷³ La_{Sn} is low-energy and can compensate $\text{La}_{\text{Ba}}^{\bullet}$, so this is certainly a possibility.⁵⁴ Despite the larger size of Pr^{3+} compared to Nd^{3+} , Pr-doped films have comparable, and perhaps lower, mobilities than Nd-doped films. Pr^{4+} can exist and substitute for Sn^{4+} as we have discussed, so that is one potential mechanism for the lower conduction and additional band in the ellipsometry data for Pr-doped films. There is also some evidence for the existence of Pr^{4+} in SQUID magnetometry and XMCD.

With respect to magnetic doping, it appears that Gd- and Nd-doping are more promising than Pr for this reason. Both Gd and Nd are stable in the trivalent state, which is more desirable so as to maximize S . Though the dopants led to paramagnetism and there is no evidence for long-range order, there is some room for improvement. Because the slope of the n versus μ curve is positive, we reason that it is possible to both increase the conductivity by adding more dopants while also increasing magnetic response.

V. CONCLUSION

In summary, we have demonstrated transparency, high mobility and paramagnetism in 8% Pr-, Nd- and Gd-doped epitaxial BaSnO_3 thin films. The larger the dopant size mismatch with the Ba-site, the smaller carrier concentrations and electron mobilities. The crystallinity of the thin film samples does not appear to be main limiter of the electron mobilities, and we have also shown that in PLD-grown BaSnO_3 films, the mean free path is smaller than the grain size. Both bulk magnetometry and XMCD measurements show that these epitaxial films exhibit strong paramagnetic signals with no evidence of long-range order. The positive trend of magnetic dopant concentrations with carrier mobilities in all rare-earth doped films in this study shows that opportunities remain to increase *both* the mobility and the magnetization in these films with higher doping concentrations in the quest toward a new class of ferromagnetic semiconductors.

VI. ACKNOWLEDGMENTS

We thank Purnima P. Balakrishnan, Charles L. Flint, Matthew T. Gray, Michael J. Veit and Useong Kim for

useful discussions. This work was supported by the National Science Foundation on Award No. 1762971. Part of this work was performed at the Stanford Nano Shared Facilities (SNSF), supported by the National Science Foundation under Award No. ECCS-1542152. Additional support was granted by the Chemical Imaging Initiative, a Laboratory Directed Research and Development Program at Pacific Northwest National Laboratory (PNNL). PNNL is a multi-program national laboratory operated by Battelle for the U.S. Department of Energy

(DOE) under Contract No. DE-AC05-76RL01830. A portion of the research was performed using the Environmental Molecular Sciences Laboratory (EMSL), a national scientific user facility sponsored by the Department of Energy's Office of Biological and Environmental Research and located at PNNL. RBS was carried out in the Characterization Facility, University of Minnesota, which receives partial support from NSF through the MRSEC program. This research used resources of the Advanced Light Source, which is a DOE Office of Science User Facility under contract no. DE-AC02-05CH11231.

-
- * usalaan@gmail.com
- ¹ K. Ohnishi, T. and Shibuya, T. Yamamoto, and M. Lippmaa. Defects and transport in complex oxide thin films. *J. Appl. Phys.*, 103:1–6, 2008.
 - ² J. Son, P. Moetakef, B. Jalan, O. Bierwagen, N. J. Wright, R. Engel-Herbert, and S. Stemmer. Epitaxial SrTiO₃ films with electron mobilities exceeding 30,000 cm²V⁻¹s⁻¹. *Nature Mater.*, 9(6):482–484, 2010.
 - ³ E. T. Tsymbal, E. Dagotto, C. B. Eom, and R. Ramesh, editors. *Multifunctional Oxide Heterostructures*. Oxford University Press, Oxford, Oxford, 2012.
 - ⁴ S. Ismail-Beigi, F. J. Walker, S.-W. Cheong, K. M. Rabe, and C. H. Ahn. Alkaline earth stannates: The next silicon? *APL Mater.*, 3(6):62510, 2015.
 - ⁵ Tyler A. Cain, Adam P. Kajdos, and Susanne Stemmer. La-doped SrTiO₃ films with large cryogenic thermoelectric power factors. *Applied Physics Letters*, 102(18), 2013.
 - ⁶ X. Luo, Y. S. Oh, A. Sirenko, P. Gao, T. A. Tyson, K. Char, and S.-W. Cheong. High carrier mobility in transparent Ba_{1-x}La_xSnO₃ crystals with a wide band gap. *Appl. Phys. Lett.*, 100:172112, 2012.
 - ⁷ H. J. Kim, U. Kim, H. M. Kim, T. H. Kim, H. S. Mun, B.-G. Jeon, K. T. Hong, W.-J. Lee, C. Ju, Kee Hoon Kim, and K. Char. High mobility in a stable transparent perovskite oxide. *Appl. Physics Exp.*, 5(6):061102, 2012.
 - ⁸ H. J. Kim, U. Kim, T. H. Kim, J. Kim, H. M. Kim, B. G. Jeon, W. J. Lee, H. S. Mun, K. T. Hong, Jaejun Yu, K. Char, and K. H. Kim. Physical properties of transparent perovskite oxides (Ba,La)SnO₃ with high electrical mobility at room temperature. *Phys. Rev. B*, 86(16):165205, 2012.
 - ⁹ Woong-Jhae Lee, Hyung Joon Kim, Jeonghun Kang, Dong Hyun Jang, Tai Hoon Kim, Jeong Hyuk Lee, and Kee Hoon Kim. Transparent Perovskite Barium Stannate with High Electron Mobility and Thermal Stability. *Annu. Rev. Mater. Res.*, 47:391–423, 2017.
 - ¹⁰ Santosh Raghavan, Timo Schumann, Honggyu Kim, Jack Y. Zhang, Tyler A. Cain, and Susanne Stemmer. High-mobility BaSnO₃ grown by oxide molecular beam epitaxy. *APL Mater.*, 4(1):1–6, 2016.
 - ¹¹ Hanjong Paik, Zhen Chen, Edward Lochocki, H. Ariel Seidner, Amit Verma, Nicholas Tanen, Jisung Park, Masaki Uchida, Shunli Shang, Bi Cheng Zhou, Mario Brützmam, Reinhard Uecker, Zi Kui Liu, Debdeep Jena, Kyle M. Shen, David A. Muller, and Darrell G. Schlom. Adsorption-controlled growth of La-doped BaSnO₃ by molecular-beam epitaxy. *APL Materials*, 5(11), 2017.
 - ¹² A. Prakash, P. Xu, A. Faghaninia, S. Shukla, J. W. Ager III, C. S. Lo, and B. Jalan. Wide bandgap BaSnO₃ films with room temperature conductivity exceeding 104 S cm⁻¹. *Nature Comm.*, 8:15167, 2017.
 - ¹³ Z. Lebens-Higgins, D. O. Scanlon, H. Paik, S. Sallis, Y. Nie, M. Uchida, N. F. Quackenbush, M. J. Wahila, G. E. Sterbinsky, Dario A. Arena, J. C. Woicik, D. G. Schlom, and L. F. J. Piper. Direct Observation of Electrostatically Driven Band Gap Renormalization in a Degenerate Perovskite Transparent Conducting Oxide. *Phys. Rev. Lett.*, 116(2):027602, 2016.
 - ¹⁴ O. Parkash, D. Kumar, K. K. Srivastav, and R. K. Dwivedi. Electrical conduction behaviour of cobalt substituted BaSnO₃. *J. Mater. Science*, 36:5805–5810, 2001.
 - ¹⁵ K. Balamurugan, N. H. Kumar, J. A. Chelvane, and P. N. Santhosh. Room temperature ferromagnetism in Fe-doped BaSnO₃. *J. Alloys Comp.*, 472(1-2):9–12, 2009.
 - ¹⁶ K. Balamurugan, N. Harish Kumar, B. Ramachandran, M. S. Ramachandra Rao, J. Arout Chelvane, and P. N. Santhosh. Magnetic and optical properties of Mn-doped BaSnO₃. *Solid State Comm.*, 149(21-22):884–887, 2009.
 - ¹⁷ Qinzhuang Liu, Yunhua He, Hong Li, Bing Li, Guanyin Gao, Lele Fan, and Jianming Dai. Room-temperature ferromagnetism in transparent Mn-doped BaSnO₃ epitaxial films. *Appl. Physics Exp.*, 7:033006, 2014.
 - ¹⁸ K.K. James and M.K. Aravind, A. and Jayaraj. Structural, optical and magnetic properties of Fe-doped barium stannate thin films grown by PLD. *Appl. Surf. Science*, 282:121–125, 2013.
 - ¹⁹ U. S. Alaan, A. T. N'Diaye, P. Shafer, E. Arenholz, and Y. Suzuki. Structure and magnetism of Fe-doped BaSnO₃ thin films. *AIP Advances*, 7(5):1–8, 2017.
 - ²⁰ Dong Sheng Gao, Xiang Dong Gao, Yong Qing Wu, Tong Tong Zhang, Jing Nan Yang, and Xiao Min Li. Epitaxial Co-doped BaSnO₃ thin films with tunable optical bandgap on MgO substrate. *Appl. Physics A: Mater. Science Processing*, 125(3):1–8, 2019.
 - ²¹ J. M. D. Coey, A. P. Douvalis, C. B. Fitzgerald, and M. Venkatesan. Ferromagnetism in Fe-doped SnO₂ thin films. *Appl. Phys. Lett.*, 84:1332, 2004.
 - ²² K Balamurugan, N Harish Kumar, J Arout Chelvane, and P N Santhosh. Effect of W co-doping on the optical, magnetic and electrical properties of Fe-doped BaSnO₃. *Physica B: Cond. Matt.*, 407(13):2519–2523, 2012.
 - ²³ U. S. Alaan, P. Shafer, A. T. N'Diaye, E. Arenholz, and Y. Suzuki. Gd-doped BaSnO₃: A transparent conducting oxide with localized magnetic moments. *Appl. Phys. Lett.*,

- 108:042106, 2016.
- ²⁴ E. McCalla, D. Phelan, M. J. Krogstad, B. Dabrowski, and C. Leighton. Electrical Transport, Magnetic and Thermodynamic Properties of La, Pr and Nd Doped BaSnO_{3-δ} Single Crystals. *Phys. Rev. Mater.*, 2:84601, 2018.
- ²⁵ Fang-Yuan Fan, Wei-Yao Zhao, Ting-Wei Chen, Jian-Min Yan, Jin-Peng Ma, Lei Guo, Guan-Yin Gao, Fei-Fei Wang, and Ren-Kui Zheng. Excellent structural, optical, and electrical properties of Nd-doped BaSnO₃ transparent thin films. *Appl. Phys. Lett.*, 113:202102, 2018.
- ²⁶ While the films are generally of good quality, there were some cases where other phases occurred. Most notably, a small peak may appear in between the film and substrate 002 reflections near ~45°. We attribute this to the 002 or 202 Ba₂SnO₄ phase. For some depositions, a BSO 111 reflection was also observed. There did not appear to be a correlation with the observation of these secondary phases; they appeared occasionally in all doping schemes.
- ²⁷ R. D. Shannon and C. T. Prewitt. Effective ionic radii in oxides and fluorides. *Acta Crystallographica Sect. B*, 25(5):925–946, 1969.
- ²⁸ R. D. Shannon. Revised effective ionic radii and systematic studies of interatomic distances in halides and chalcogenides. *Acta Crystallographica Sect. A*, 32(5):751–767, 1976.
- ²⁹ Y. Q. Jia. Crystal radii and effective ionic radii of the rare earth ions. *J. Solid State Chem.*, 95(1):184–187, 1991.
- ³⁰ T. Huang and M. Itoh. Electrical properties of BaSnO₃ in substitution of antimony for tin and lanthanum for barium. *J. Mater. Science*, 30:1556–1560, 1995.
- ³¹ M. Leszczyński, E. Litwin-Staszewska, T. Suski, J. Bak-Misiuk, and J. Domagala. Lattice Constant of Doped Semiconductor. *Acta Physica Polonica A*, 88(5):837–840, 1995.
- ³² P. V. Wadekar, J. Alaria, M. O’Sullivan, N. L O Flack, T. D. Manning, L. J. Phillips, K. Durose, O. Lozano, S. Lucas, J. B. Claridge, and M. J. Rosseinsky. Improved electrical mobility in highly epitaxial La:BaSnO₃ films on SmScO₃(110) substrates. *Appl. Phys. Lett.*, 105(5):101–105, 2014.
- ³³ M. G. Smith, J. B. Goodenough, A. Manthiram, R. D. Taylor, Weimin Peng, and C. W. Kimball. Tin and Antimony Valence States in BaSn_{0.85}Sb_{0.15}O_{3-δ}. *J. Solid State Chem.*, 98:181–186, 1992.
- ³⁴ Mohamed Trari, Jean-Pierre Doumerc, Patrice Dordor, Michel Pouchard, Günter Behr, and Gernot Krabbes. Preparation and characterization of lanthanum-doped BaSnO₃. *J. Phys. Chem. Solids*, 55(11):3–7, 1994.
- ³⁵ B. Hadjarab, A. Bouguelia, and M. Trari. Optical and transport properties of lanthanum-doped stannate BaSnO₃. *J. Physics D: Appl. Physics*, 40(19):5833–5839, 2007.
- ³⁶ M. Yasukawa, T. Ikeuchi, K. and Kono, H. Yanagi, and H. Hosono. Preparation of semiconductive La-doped BaSnO₃ by a polymerized complex method and the thermoelectric properties. *J. Jpn. Soc. Powder Metallurgy*, 54(9):639–644, 2007.
- ³⁷ H. F. Wang, Q. Z. Liu, F. Chen, G. Y. Gao, W. Wu, and X. H. Chen. Transparent and conductive oxide films with the perovskite structure: La- and Sb-doped BaSnO₃. *J. Appl. Phys.*, 101(10):106105, 2007.
- ³⁸ D. Y. Wang, J. Wang, H. L. W. Chan, and C. L. Choy. Structural and electro-optic properties of Ba_{0.7}Sr_{0.3}TiO₃ thin films grown on various substrates using pulsed laser deposition. *J. Appl. Phys.*, 101(4):043515, 2007.
- ³⁹ B. Hadjarab, A. Bouguelia, A. Benchettara, and M. Trari. The transport and photo electrochemical properties of La-doped BaSnO₃. *J. Alloys Comp.*, 461:360–366, 2008.
- ⁴⁰ M. Yasukawa, T. Kono, K. Ueda, H. Yanagi, and H. Hosono. High-temperature thermoelectric properties of La-doped BaSnO₃ ceramics. *Materials Science & Engineering B*, 173(1-3):29–32, 2010.
- ⁴¹ Q. Liu, J. Liu, B. Li, H. Li, G. Zhu, Kai Dai, Z. Liu, P. Zhang, and J. Dai. Composition dependent metal-semiconductor transition in transparent and conductive La-doped BaSnO₃ epitaxial films. *Appl. Phys. Lett.*, 101(24):241901, 2012.
- ⁴² K. K. James, P. S. Krishnaprasad, K. Hasna, and M. K. Jayaraj. Structural and optical properties of La-doped BaSnO₃ thin films grown by PLD. *J. Physics Chem. Solids*, 76:64–69, 2015.
- ⁴³ Useong Kim, Chulkwon Park, Taewoo Ha, Young Mo Kim, Namwook Kim, Chanjong Ju, Jisung Park, Jaejun Yu, Jae Hoon Kim, and Kookrin Char. All-perovskite transparent high mobility field effect using epitaxial BaSnO₃ and LaInO₃. *APL Materials*, 3(3):0–7, 2015.
- ⁴⁴ R. H. Wei, X. W. Tang, Z. Z. Hui, X. Luo, J. M. Dai, J. Yang, W. H. Song, L. Chen, X. G. Zhu, X. B. Zhu, and Y. P. Sun. Solution processing of transparent conducting epitaxial La:BaSnO₃ films with improved electrical mobility. *Applied Physics Letters*, 106(10):2–7, 2015.
- ⁴⁵ Woong-Jhae Lee, Hyung Joon Kim, Egon Sohn, Tai Hoon Kim, Ju-Young Park, Woanse Park, Hyunhak Jeong, Takhee Lee, Jin Hyeok Kim, Ki-Young Choi, and Kee Hoon Kim. Enhanced electron mobility in epitaxial (Ba,La)SnO₃ films on BaSnO₃(001) substrates. *Applied Physics Letters*, 108(8):082105, 2016.
- ⁴⁶ J. Shiogai, K. Nishihara, and A. Sato, K. and Tsukazaki. Improvement of electron mobility in La:BaSnO₃ thin films by insertion of an atomically flat insulating (Sr,Ba)SnO₃ buffer layer. *AIP Advances*, 6:065305, 2016.
- ⁴⁷ Sangbae Yu, Daseob Yoon, and Junwoo Son. Enhancing electron mobility in La-doped BaSnO₃ thin films by thermal strain to annihilate extended defects. *Applied Physics Letters*, 108(26):262101, 2016.
- ⁴⁸ Christian A. Niedermeier, Sneha Rhode, Sarah Fearn, Keisuke Ide, Michelle A. Moram, Hidenori Hiramatsu, Hideo Hosono, and Toshio Kamiya. Solid phase epitaxial growth of high mobility La:BaSnO₃ thin films codoped with interstitial hydrogen. *Applied Physics Letters*, 108(17):172101, 2016.
- ⁴⁹ K. Ganguly, B. Prakash, A. and Jalan, and C. Leighton. Mobility-electron density relation probed via controlled oxygen vacancy doping in epitaxial BaSnO₃. *APL Mater.*, 056102:1–7, 2017.
- ⁵⁰ Christian A. Niedermeier, Sneha Rhode, Keisuke Ide, Hidenori Hiramatsu, Hideo Hosono, Toshio Kamiya, and Michelle A. Moram. Electron effective mass and mobility limits in degenerate perovskite stannate BaSnO₃. *Physical Review B Rapid Communications*, 95:161202(R), 2017.
- ⁵¹ Yusuke Ozaki, Daisuke Kan, and Yuichi Shimakawa. Influence of cation off-stoichiometry on structural and transport properties of (Ba,La)SnO₃ epitaxial thin films grown by pulsed laser deposition. *Journal of Applied Physics*, 121(21):215304, 2017.
- ⁵² Abhinav Prakash, Peng Xu, Xuewang Wu, Greg Haugstad, Xiaojia Wang, and Bharat Jalan. Adsorption-controlled growth and the influence of stoichiometry on electronic transport in hybrid molecular beam epitaxy-grown

- BaSnO₃ films. *J. Mater. Chem. C*, 5:5730–5736, 2017.
- ⁵³ Koustav Ganguly, Palak Ambwani, Peng Xu, Jong Seok Jeong, K Andre Mkhoyan, Christopher Leighton, and Bharat Jalan. Structure and transport in high pressure oxygen sputter-deposited BaSnO_{3-δ}. *APL Mater.*, 3(6):62509, 2015.
- ⁵⁴ D. O. Scanlon. Defect engineering of BaSnO₃ for high-performance transparent conducting oxide applications. *Phys. Rev. B*, 87(16):161201(R), 2013.
- ⁵⁵ Useong Kim, Chulkwon Park, Taewoo Ha, Rokyoon Kim, Hyo Sik Mun, Hoon Min Kim, Hyung Joon Kim, Tai Hoon Kim, Namwook Kim, Jaejun Yu, Kee Hoon Kim, Jae Hoon Kim, and Kookrin Char. Dopant-site-dependent scattering by dislocations in epitaxial films of perovskite semiconductor BaSnO₃. *APL Mater.*, 2(5):56107, 2014.
- ⁵⁶ J. Herrero-Martín, J. L. García-Muñoz, S. Valencia, C. Frontera, J. Blasco, A. Barón-González, G. Subías, R. Abrudan, F. Radu, E. Dudzik, and R. Feyerherm. Valence change of praseodymium in Pr_{0.5}Ca_{0.5}CoO₃ investigated by x-ray absorption spectroscopy. *Phys. Rev. B*, 84:115131, 2011.
- ⁵⁷ F. Guillou, Q. Zhang, Z. Hu, C. Y. Kuo, Y. Y. Chin, H. J. Lin, C. T. Chen, A. Tanaka, L. H. Tjeng, and V. Hardy. Coupled valence and spin state transition in (Pr_{0.7}Sm_{0.3})_{0.7}Ca_{0.3}Co₃. *Phys. Rev. B*, 87(11):115114, 2013.
- ⁵⁸ F. Guillou, Y. Bréard, and V. Hardy. Cobalt spin state above the valence and spin-state transition in (Pr_{0.7}Sm_{0.3})_{0.7}Ca_{0.3}CoO₃. *Solid State Sciences*, 24:120–124, 2013.
- ⁵⁹ Jessica Padilla-Pantoja, Javier Herrero-Martín, Pierluigi Gargiani, S Manuel Valvidares, Vera Cuartero, Kurt Kummer, Oliver Watson, Nicholas B Brookes, and José Luis García-Muñoz. Stability of the Cationic Oxidation States in Pr_{0.50}Sr_{0.50}CoO₃ across the Magnetostructural Transition by X-ray Absorption Spectroscopy. *Inorg. Chem.*, 53:8854–8858, 2014.
- ⁶⁰ M. Bickel, G. L. Goodman, L. Soderholm, and B. Kanelakopoulos. The magnetic susceptibility of Pr⁴⁺ in BaPrO₃: Evidence of long-range magnetic order. *J. Solid State Chem.*, 76:178–185, 1988.
- ⁶¹ M. N. Popova, S. A. Klimin, B. Z. Malkin, L. A. Kasatkina, G. Cao, and J. Crow. Crystal field and spectrum of Pr⁴⁺ in BaPrO₃. *Phys. Lett. A*, 223:308–312, 1996.
- ⁶² Y. Hinatsu and N. Edelstein. Electron Paramagnetic Resonance Spectrum of Pr⁴⁺ in BaCeO₃. *J. Solid State Chem.*, 112:53–57, 1994.
- ⁶³ Y. Hinatsu. Electron Paramagnetic Resonance Spectra of Pr⁴⁺ in BaCeO₃, BaZrO₃, BaSnO₃, and Their Solid Solutions. *J. Solid State Chem.*, 122:384–389, 1996.
- ⁶⁴ Keitaro Tezuka and Yukio Hinatsu. Electron Paramagnetic Resonance Study of Pr⁴⁺ Ions Doped in BaHfO₃ Perovskite. *J. Solid State Chem.*, 156:203–206, 2001.
- ⁶⁵ B. T. Thole, G. van der Laan, J. C. Fuggle, G. A. Sawatzky, R. C. Karnatak, and J. M. Esteve. 3d x-ray-absorption lines and the 3d⁹4fⁿ⁺¹ multiplets of the lanthanides. *Phys. Rev. B*, 32(8):5107–5118, 1985.
- ⁶⁶ J. B. Goedkoop, B. T. Thole, G. van der Laan, G. A. Sawatzky, F. M. F. de Groot, and J. C. Fuggle. Calculations of magnetic x-ray dichroism in the 3d absorption spectra of rare-earth compounds. *Phys. Rev. B*, 37:2086–2093, 1988.
- ⁶⁷ J. B. Goedkoop. *X-Ray Dichroism of Rare Earth Materials*. Doctoral dissertation, Ketholieke Universiteit te Nijmegen, 1989.
- ⁶⁸ S. Sallis, D. O. Scanlon, S. C. Chae, N. F. Quackenbush, D. A. Fischer, J. C. Woicik, J.-H. Guo, S. W. Cheong, and L. F. J. Piper. La-doped BaSnO₃—Degenerate perovskite transparent conducting oxide: Evidence from synchrotron x-ray spectroscopy. *Appl. Phys. Lett.*, 103:042105, 2013.
- ⁶⁹ S. A. Chambers, T. C. Kaspar, Abhinav Prakash, Greg Haugstad, and Bharat Jalan. Band alignment at epitaxial BaSnO₃/SrTiO₃(001) and BaSnO₃/LaAlO₃(001) heterojunctions. *Appl. Phys. Lett.*, 108(15):1–5, 2016.
- ⁷⁰ P. P. Balakrishnan, M. J. Veit, U. S. Alaán, M. T. Gray, and Yuri Suzuki. Metallicity in SrTiO₃ substrates induced by pulsed laser deposition. *APL Materials*, 7(1), 2019.
- ⁷¹ E. Holmelund, J. Schou, S. Tougaard, and N. B. Larsen. Pure and Sn-doped ZnO films produced by pulsed laser deposition. *Appl. Surf. Sci.*, 197-198:467–471, 2002.
- ⁷² B Hadjarab, M Trari, and M Kebir. Physical characterization of the semiconducting deficient perovskite BaSnO_{3-δ}. *Mater. Sci. Semi. Processing*, 29:283–287, 2015.
- ⁷³ The theoretical prediction states that this type of defect occurs in oxygen-rich, metal-poor scenarios. This would be the opposite of our observations once again; for us, higher oxygen pressures lead to lower conductivities. As we discussed previously, it may be significant that the defect has a low formation energy, even if the exact conditions of the activation are at odds between our results and their theoretical predictions. Alternatively, growth in low oxygen pressures may not constitute ‘oxygen-poor’ conditions due either to complications with PLD growth or a stringent definition of ‘rich’ and ‘poor’ in the theoretical study.⁵⁴